Density-functional study of undoped and doped *trans*-polyacetylene

J. Paloheimo
Semiconductor Laboratory, Technical Research Centre of Finland, SF-02150 Espoo, Finland

J. von Boehm
Laboratory of Computational Dynamics, Helsinki University of Technology, SF-02150 Espoo, Finland
(Received 19 April 1993)

We report a self-consistent linear-combination-of-Gaussian-orbitals study of the electronic states and ground-state geometry of an undoped and doped single, infinite chain of *trans*-polyacetylene using the density-functional theory in the local-density approximation. We find a dimerized ground state for an undoped chain with a dimerization amplitude of about 0.01 Å, which is lower than the experimental value of 0.023–0.03 Å. A pure Hartree calculation neglecting all exchange and correlation gives a much smaller dimerization amplitude of less than 0.005 Å. The local exchange-correlation energy thus significantly favors the dimerization although its effect is not strong enough. In the calculations of the doped chains, the dopant ions were approximated by a uniform background charge. We find that the undimerized state becomes energetically more favorable than any uniformly dimerized state at a critical doping level of about 0.04 (0.03) extra holes (electrons) per CH unit. The band structures and total energies of polaron and soliton lattices at a higher doping level of 0.2 holes per CH unit are calculated and compared with those of the uniformly dimerized and undimerized lattices, and possible models of the metallic state of *trans*-polyacetylene are discussed. According to our study, the bonds become increasingly similar with increasing doping. The undimerized chain model seems to be a good approximation for the metallic state of *trans*-polyacetylene at high doping levels although the possibility for a marginal soliton lattice cannot be fully excluded.

I. INTRODUCTION

Trans-polyacetylene is the prototype of all quasi-one-dimensional conducting polymers.[1,2] The experimental gap of undoped *trans*-polyacetylene consisting of interacting chains is about 1.4–1.5 eV.[3] An undoped single *trans*-polyacetylene chain is expected to have a gap of about 1.7–1.8 eV. *Trans*-polyacetylene differs from three-dimensional symmetric inorganic semiconductors, such as silicon, in that the anisotropic lattice structure of *trans*-polyacetylene is easily modified by electron-phonon coupling leading to a dimerized ground state with alternating single and double bonds and to self-localization of extra charges into solitons and polarons.[1] Although *trans*-polyacetylene is an insulator in its undoped form, the conductivity increases with increasing doping. At a doping level of about 6% per CH unit, *trans*-polyacetylene undergoes a transition into a metallic state characterized by a high density of states (DOS) at the Fermi level.[4–6] The conductivity of highly doped, well-ordered *trans*-polyacetylene may exceed 10^5 S/cm at room temperature.[7]

The studies of *trans*-polyacetylene and other conducting polymers are motivated by their interesting physical phenomena and the potential conducting polymers may have to applications that range from electromagnetic interference shielding to molecular electronics.[2] Theoretists have favored *trans*-polyacetylene over other conducting polymers because of its simple molecular structure. Although *trans*-polyacetylene itself is probably not going to become commercially important because of its poor stability, there are already commercial applications of some other conducting polymers. Many biologically important macromolecules such as β-carotene also have conjugated structures.

Experiments using the x-ray diffraction technique[8,9] and nutation NMR spectroscopy[10] have shown that undoped *trans*-polyacetylene has a dimerized ground state. Although the dimerization is a very basic phenomenon, it is still not fully understood. The dimerization has been mostly discussed in the context of simple tight-binding models, but there is no general agreement of the relative importance of the electron-phonon and the electron-electron interactions (see Ref. 11 and references therein). Confusion has also arisen because the self-consistent (SC) first-principles Hohenberg-Kohn-Sham (HKS) density-functional (DF) calculations using the local-density approximation (LDA) for the exchange-correlation energy have given conflicting results for the dimerization of an undoped infinite *trans*-polyacetylene chain. These results range from a dimerization close to experiments[12,13] to a weak dimerization[14–18] or no dimerization at all.[19]

Contrary to the undoped case, there are no direct measurements of the chain geometry in the highly doped metallic state. Theoretical considerations and experiments have shown that the charge in lightly doped *trans*-polyacetylene is mostly stored into spinless localized solitons,[1] but, on the other hand, the chain geometry in the highly doped metallic state is not known. The measured abrupt increase in the Pauli spin susceptibility at a doping level of about 6% per CH unit is the most dramatic change.[4,5] The same characteristics are found for *p*-type

0163-1829/93/48(23)/16948(17)/$06.00

doping (ClO_4^- ions) and for n-type doping (Na^+ ions). The experimental Pauli spin susceptibility[4,5] and the electronic specific heat[6] of the highly doped samples indicate a high metallic DOS at the Fermi energy: $g(E_F)\simeq 0.08-0.12$ states/eV/carbon atom. The remarkable conductivity of about 10^5 S/cm in the best samples[7] suggests a mean free path of about 100 Å.[20] The temperature dependence is still mostly nonmetallic, the conductivity decreasing with decreasing temperature, but still remaining large when approaching zero temperature.[7] Transport models considering conducting metallic islands separated by thin barriers have been successful for explaining these characteristics. However, some samples have even shown signs of metallic temperature dependence at high temperatures, suggesting that there is a contribution from the intrinsic optical-phonon-scattering-limited conductivity in the metallic chains.[7,20] The optical (infrared) spectra of highly doped *trans*-polyacetylene[5,21] resemble those of a simple metal. On the other hand, the infrared active vibrational (IRAV) modes indicating the presence of localized defects[22] (e.g., solitons or polarons) at low doping levels, persist up to the highest doping levels,[23] thereby suggesting nonuniformities in the electron density at the highest doping levels, too. The metallic state has been actively studied theoretically and the following models explaining the physical properties have been suggested: a soliton lattice or an incommensurate Peierls state (the latter corresponding to a dense soliton lattice),[5,24–29] a polaron lattice,[30,31] and an undimerized chain.[20,32,33]

The purpose of this paper is to present a comprehensive study of various electronic and structural properties of undoped and doped *trans*-polyacetylene. Some parts of this paper have appeared in other works.[18,33] We use a SC linear-combination-of-Gaussian-orbitals (LCGO) method[34] in the HKS DF theory in the LDA. This paper has the following format. In Sec. II we present our methods. The results are presented and discussed in Sec. III. The conclusions are drawn in Sec. IV.

II. METHODS

A. Formalism

The HKS DF formalism[35,36] is based on the fact that the total energy of the interacting electron-nuclear system can be written in the form

$$E[\rho(\mathbf{r})]=\int V_{\rm ext}(\mathbf{r})\rho(\mathbf{r})d^3r+G[\rho(\mathbf{r})]\ , \tag{1}$$

where $\rho(\mathbf{r})$ is the electron density, $V_{\rm ext}(\mathbf{r})$ is an external potential including the electron-nuclear and internuclear interactions, and $G[\rho(\mathbf{r})]$ is a universal functional of $\rho(\mathbf{r})$, independent of $V_{\rm ext}$. The functional $E[\rho(\mathbf{r})]$ attains its minimum value for the true ground state $\rho(\mathbf{r})$. Variation of $E[\rho(\mathbf{r})]$ with respect to $\rho(\mathbf{r})$ leads to effective one-electron Schrödinger equations (Hartree atomic units are used throughout)

$$\left[-\frac{1}{2}\nabla^2-\sum_p\frac{Z_p}{|\mathbf{r}-\mathbf{r}_p|}+\int\frac{\rho(\mathbf{r})}{|\mathbf{r}-\mathbf{r}'|}d^3+\frac{\delta E_{\rm xc}[\rho(\mathbf{r})]}{\delta\rho(\mathbf{r})}\right]\Psi_j(\mathbf{r})=\varepsilon_j\Psi_j(\mathbf{r})\ , \tag{2}$$

where Z_p is the charge of the nucleus at $\mathbf{r}_p$, $E_{\rm xc}[\rho(\mathbf{r})]$ is the total exchange-correlation energy of the HKS formalism, and the eigenfunctions Ψ_j determine further the density

$$\rho(\mathbf{r})=2\sum_j^{\rm occ}\Psi_j(\mathbf{r})^*\Psi_j(\mathbf{r}) \tag{3}$$

(the non-spin-polarized case is assumed). The Ψ_j's are calculated from Eqs. (2) and (3) by using SC iteration. E is then given by the expression

$$E=2\sum_j^{\rm occ}\langle\Psi_j|-\tfrac{1}{2}\nabla^2\Psi_j\rangle+E_{\rm xc}[\rho(\mathbf{r})]+\int\rho(\mathbf{r})\left[-\sum_p\frac{Z_p}{|\mathbf{r}-\mathbf{r}_p|}+\frac{1}{2}\int\frac{\rho(\mathbf{r}')}{|\mathbf{r}-\mathbf{r}'|}d^3\mathbf{r}'\right]d^3r+\sum_{p<q}\sum\frac{Z_pZ_q}{|\mathbf{r}_p-\mathbf{r}_q|}\ , \tag{4}$$

where we use for $E_{\rm xc}[\rho(\mathbf{r})]$ and for the effective exchange-correlation potential $V_{\rm xc}=\delta E_{\rm xc}[\rho(\mathbf{r})]/\delta\rho(\mathbf{r})$ in Eq. (2) the LDA model based on the calculations by Ceperley and Alder[37] and parametrized by Perdew and Zunger.[38]

The density is divided into two parts[34,39]

$$\rho=\rho_0+\Delta\rho\ , \tag{5}$$

where ρ_0 consists of fixed spherically symmetric pseudoatomic densities compensating the nuclear charges

$$\rho_0(\mathbf{r})=\sum_p\rho_0^p(|\mathbf{r}-\mathbf{r}_p|)\ , \tag{6}$$

$$\int\rho_0^p(r)d^3r=Z_p\ , \tag{7}$$

and the deformation density $\Delta\rho$ is neutral

$$\int\Delta\rho(\mathbf{r})d^3r=0\ . \tag{8}$$

$\Delta\rho$ is relatively smooth and has the symmetry of the crystal. Therefore, $\Delta\rho$ is expanded in terms of plane waves

$$\Delta\rho=\sum_{\mathbf{G}\,(\neq 0)}\Delta\rho(\mathbf{G})e^{-i\mathbf{G}\cdot\mathbf{r}}\ , \tag{9}$$

where $\mathbf{G}$ denotes reciprocal-lattice vectors.

The division of ρ [Eq. (5)] divides the effective crystal potential $V=V_C+V_{\rm xc}$ [V_C is the Coulombic part consisting of the second and third terms in Eq. (2)] into the corresponding parts

$$V=V_0+\Delta V\ . \tag{10}$$

The pseudoatomic part V_0 consists of spherically symmetric functions

$$V_0(\mathbf{r})=\sum_pV_0^p(|\mathbf{r}-\mathbf{r}_p|)\ . \tag{11}$$

The $V_0^p(r)$'s are calculated from the expression

$$V_0^p=-\frac{Z_p}{r}+4\pi\left[\frac{1}{r}\int_0^r r'^2\rho_0^p(r')dr'+\int_r^\infty r'\rho_0^p(r')dr'\right]+V_{\rm xc}[\rho_0^p(r)] \tag{12}$$

and are further expanded in terms of Gaussians

$$V_0^p(r)=-\frac{Z_p}{r}e^{-\alpha_1 r^2}+\sum_{j=2}^{M}c_j e^{-\alpha_j r^2}\ . \tag{13}$$

The relatively smooth ΔV having the symmetry of the crystal is expanded in terms of plane waves

$$\Delta V(\mathbf{r})=\sum_{\mathbf{G}}\Delta V(\mathbf{G})e^{-i\mathbf{G}\cdot\mathbf{r}}\ . \tag{14}$$

The Coulombic parts of the Fourier coefficients are obtained from Poisson's equation

$$\Delta V_C(\mathbf{G})=\frac{4\pi}{G^2}\Delta\rho(\mathbf{G})\ ,\quad \mathbf{G}\neq\mathbf{0} \tag{15}$$

and from the approximation[40]

$$\Delta V_C(\mathbf{G}=0)=-\frac{2\pi}{3\Omega_0}\int_{\Omega_0}\Delta\rho(\mathbf{r})r^2d^3r\ , \tag{16}$$

where Ω_0 is the volume of the primitive unit cell. The Fourier coefficients

$$\Delta\rho(\mathbf{G})=\frac{1}{\Omega_0}\int_{\Omega_0}[\rho(\mathbf{r})-\rho_0(\mathbf{r})]e^{i\mathbf{G}\cdot\mathbf{r}}d^3r \tag{17}$$

and

$$\Delta V_{\rm xc}(\mathbf{G})=\frac{1}{\Omega_0}\int_{\Omega_0}\left\{V_{\rm xc}[\rho(\mathbf{r})]-\sum_p V_{\rm xc}[\rho_0^p(|\mathbf{r}-\mathbf{r}_p|)]\right\}e^{i\mathbf{G}\cdot\mathbf{r}}d^3r \tag{18}$$

are calculated using a fine regular mesh in the primitive unit cell.

The eigenfunctions of Eq. (2) are expanded in terms of Bloch basis functions as follows:

$$\Psi_{\mathbf{k}}=\sum_i\varphi_{\mathbf{k}i}c_{\mathbf{k}i}\ . \tag{19}$$

In this equation

$$\varphi_{\mathbf{k}i}=\frac{1}{\sqrt{N}}\sum_m e^{i\mathbf{k}\cdot\mathbf{R}_m}\chi_i(\mathbf{r}-\mathbf{R}_m-\tau_i)\ , \tag{20}$$

where N is the number of primitive unit cells in the region defined by the periodic boundary conditions, $\mathbf{R}_m$ is a primitive lattice vector, τ_i is the position vector of the nucleus i in the primitive unit cell, and the χ_i's are further expressed as linear combinations of Gaussian orbitals

$$\chi_i(\mathbf{r}-\tau_i)=\sum_s a_s^i G(\beta_s^i,l_s^i,m_s^i,n_s^i,\tau_s^i)\ , \tag{21}$$

$$G(\beta,l,m,n,\tau)=(x-\tau_x)^l(y-\tau_y)^m(z-\tau_z)^n e^{-\beta(\mathbf{r}-\tau)^2}\ . \tag{22}$$

The index i of χ_i labels these functions inside one primitive unit cell and with each i there is associated one specific center τ_i which always also coincides with one of the positions of the nuclei.

Substituting Eq. (19) in Eq. (2) and using the Rayleigh-Ritz variational principle gives the matrix eigenvalue equation

$$\underline{H}_{\mathbf{k}}\underline{C}_{\mathbf{k}}=\varepsilon_{\mathbf{k}}\underline{\Delta}_{\mathbf{k}}\underline{C}_{\mathbf{k}} \tag{23}$$

where the column $\underline{C}_{\mathbf{k}}$ contains the expansion coefficients $c_{\mathbf{k}i}$,

$$H_{\mathbf{k},ij}=\sum_m e^{i\mathbf{k}\cdot\mathbf{R}_m}\langle\chi_i(\mathbf{r}-\tau_i)|H\chi_j(\mathbf{r}-\mathbf{R}_m-\tau_j)\rangle \tag{24}$$

[H denotes the effective Hamiltonian of Eq. (2)], and

$$\Delta_{\mathbf{k},ij}=\sum_m e^{i\mathbf{k}\cdot\mathbf{R}_m}\langle\chi_i(\mathbf{r}-\tau_i)|\chi_j(\mathbf{r}-\mathbf{R}_m-\tau_j)\rangle\ . \tag{25}$$

The analytic or semianalytic expressions for the matrix elements between Gaussians $G(\beta,l,m,n,\tau)$ are given in Ref. 41.

The total energy is calculated as the difference between E [Eq. (4)] and the total energy of the noninteracting pseudoatoms. ΔE consists of the following parts. The Coulombic part in ΔE can be written in the form

$$\Delta E_C=A+B+C \tag{26}$$

where

$$A=4\pi N\sum_t\sum_{\mathbf{G}\,(\neq 0)}\Delta\rho(\mathbf{G})\frac{e^{-i\mathbf{G}\cdot\tau_t}}{G^2}\left[\int e^{-i\mathbf{G}\cdot\mathbf{r}}\rho_0^t(r)d^3r-Z_t\right] \tag{27}$$

accounts for the Coulombic interactions between $-\Delta\rho$ and the pseudoatom charge densities $-\rho_0^t(|\mathbf{r}-\tau_t|)+Z_t$ (t labels here the nuclei inside one primitive unit cell),

$$B=2\pi N\Omega_0\sum_{\mathbf{G}\,(\neq 0)}\frac{\Delta\rho(\mathbf{G})\Delta\rho(-\mathbf{G})}{G^2} \tag{28}$$

accounts for the Coulombic interactions between the charge densities $-\Delta\rho$ and $-\Delta\rho$, and

$$C=\sum_{p>q}\sum\int\int\frac{[\rho_0^p(|\mathbf{r}-\mathbf{r}_p|)-Z_p\delta(\mathbf{r}-\mathbf{r}_p)][\rho_0^q(|\mathbf{r}'-\mathbf{r}_q|)-Z_q\delta(\mathbf{r}'-\mathbf{r}_q)]}{|\mathbf{r}-\mathbf{r}'|}d^3r\,d^3r' \tag{29}$$

accounts for the Coulombic interactions between different pseudoatom charge densities. The kinetic-energy difference becomes

$$\Delta T = N2\sum_{n\mathbf{k}}^{\text{occ}}\sum_{i,j} c^{*}_{\mathbf{k}ni} c_{\mathbf{k}nj} \sum_{m} e^{i\mathbf{k}\cdot\mathbf{R}_m} \langle \chi_i(\mathbf{r}-\tau_i)| -\tfrac{1}{2}\nabla^2 \chi_j(\mathbf{r}-\tau_j-\mathbf{R}_m)\rangle$$
$$-N\sum_i n_{\text{occ}}(i)\langle \chi_i(\mathbf{r}-\tau_i)| -\tfrac{1}{2}\nabla^2\chi_i(\mathbf{r}-\tau_i)\rangle / \langle \chi_i(\mathbf{r}-\tau_i)|\chi_i(\mathbf{r}-\tau_i)\rangle \ , \quad (30)$$

where n is the band index and $n_{\text{occ}}(i)$ is the radial occupation number for $\chi_i(\mathbf{r}-\tau_i)$ [each radial density $\rho_0^t(\mathbf{r}-\tau_t)$ is a sum of the terms $n_{\text{occ}}(i)\chi_i(\mathbf{r}-\tau_i)^2$ which contribute to $\rho_0^t(\mathbf{r}-\tau_t)$ only when τ_i coincides with τ_t].

The exchange-correlation energy difference is calculated from the expression

$$\Delta E_{\text{xc}} = N\int_{\Omega_0}\left[\rho(\mathbf{r})\varepsilon_{\text{xc}}[\rho(\mathbf{r})] - \sum_p \rho_0^p(|\mathbf{r}-\mathbf{r}_p|)\varepsilon_{\text{xc}}[\rho_0^p(|\mathbf{r}-\mathbf{r}_p|)]\right] d^3r \ , \quad (31)$$

where ε_{xc} is the exchange-correlation energy density from Refs. 37 and 38. The total-energy difference is then

$$\Delta E = \Delta E_C + \Delta T + \Delta E_{\text{xc}} \ . \quad (32)$$

As is obvious from the above derivations our SC LCGO method uses a fully general all-electron crystal potential (no pseudopotential or muffin-tin approximation is used).

B. Doped case

Extra charges are most commonly introduced into the polymer chain by doping the polymer with suitable acceptor or donor atoms/molecules in the *p*-type or *n*-type doping, respectively, although extra carriers may also be photogenerated or injected in electronic devices.[2] The dopant counterions reside beside the polymer chains maintaining the charge neutrality of the crystal. In the calculations, we study the effect of doping by changing the number of electrons in the band states. The Fermi level, up to which the electron density $\rho(\mathbf{r})$ is integrated, is shifted so that the desired amount of extra doping charge is obtained. The absolute value of the coefficient $\Delta\rho(\mathbf{G}=0)$, calculated from $\rho(\mathbf{r})$, then equals $\delta N/\Omega_0$ (δN is the number of extra electrons per primitive unit cell of a dimer C_2H_2 having the volume Ω_0). The number of π electrons per CH unit becomes $1-y$ $(1+y)$ in the case of hole (electron) doping, where $y=|\delta N|/2$ is the doping level per CH unit. The extra electron charge δN has to be balanced by background charges. In our approach, we approximate the dopant ions by *a uniform background charge density* $\delta N/\Omega_0$, which neutralizes the system. With this small modification the equations above are still valid. The approximation should be reasonable at high doping levels because of the strong screening in the metallic state[32,42] and the overlap of the dopant potentials.[29,43]

C. Geometry

The dimerized ground state of a *trans*-polyacetylene chain is typically characterized using two parameters: the dimerization amplitude, $u=u_0$, giving the displacement $u_n=-(-1)^n u_0$ of the carbon atoms parallel to the polymer axis (x axis), and the dimerization stabilization energy per primitive unit cell, $E_S=\Delta E(u=0)-\Delta E(u=u_0)$. The polymer plane defines the x-y plane. The experimental dimerization amplitude u_0(Exp.) equals 0.023–0.03 Å and the experimental bond lengths are $r_{C=C}$(Exp.)$\simeq$1.36 Å and r_{C-C}(Exp.) $\simeq$1.44–1.45 Å.[8–10] Here $r_{C=C}$ and r_{C-C} are the bond lengths of the double and single bonds, respectively. In our calculations the C—C—C bond angles were fixed to 120°, the C—H bonds ($r_{C-H}=1.09$ Å) pointed perpendicularly to the polymer axis, and the unit cell dimensions were fixed to $a=2.434$ Å, $b=6.350$ Å, and $c=4.233$ Å. The length of the unit cell a was obtained using the bond lengths $r_{C=C}=1.36$ Å and $r_{C-C}=1.45$ Å derived from the experimental results of Ref. 9 and our fixed C—C—C angle.[44] The carbon atoms move approximately parallel to the polymer axis, the projected displacements of the two CH units in the unit cell being $+u$ and $-u$ from the undimerized sites with $x_1=-a/4$ and $x_2=+a/4$, respectively. The dimensions b and c were chosen to be wide enough to make the interchain interactions practically vanishing. Although, strictly speaking, the interactions are not totally suppressed, they are very small as $\rho(\mathbf{r})$ is practically zero in the middle between adjacent chains. The average density of π electrons in our unit cell is less than 60% of that in a normal *trans*-polyacetylene crystal, which has about $5\times10^{22}\pi$ electrons/cm^3.[8] The interchain effects decrease strongly with increasing interchain distance.[17]

D. Geometry of polaron and soliton lattices

We have also calculated, although with lower accuracy, the band structures and total energies of polaron and soliton lattices by using a large unit cell of $C_{10}H_{10}$ with the unit cell dimensions $a'=5a$, $b'=b$, and $c'=c$, where a, b, and c refer to the dimensions of the unit cell of a dimer. The large unit cell contains two charged polarons or one charged soliton and one charged antisoliton. The hole doping level was $y=20\%$. Similar undoped lattice distortions were also studied. Here, differently from the calculations assuming a unit cell of a dimer, the CH units were moved exactly parallel to the x axis (coordinates y_n were fixed at their values obtained above for the undimerized chain). The displacements of the CH units in the polaron lattice from equidistant positions x_n at high doping levels were approximated by the expression

$$u_n=-(-1)^n u_P[1+A\cos(K_P x_n+\phi)] \ , \quad (33)$$

where u_P is the average dimerization amplitude [the maximum value of $|u_n|$ is $(1+A)u_P$ and the minimum value

is $(1-A)u_P$]. A is the amplitude of the periodic modulation, assumed to be in the range 0.0–1.0. K_P defines the periodicity and ϕ the phase of the polaronic distortion. In our special case $y=20\%$, wherefore $K_P=4\pi/a'=0.8\pi/a$ and $x_n=(0.1n-0.55)a'$, $n=1,2,\ldots,10$. The sinusoidal distortion is expected to be a fairly good approximation at high y's because the polarons strongly overlap. The polaron lattice is changed into a uniformly dimerized chain if $A=0$, and an undimerized chain is obtained by setting u_P to zero.

The displacements of the CH units in the soliton lattice at large dopings may be correspondingly approximated by the expression[24]

$$u_n=-(-1)^n\frac{\pi}{2}u_S\cos(K_S x_n+\phi)\ , \tag{34}$$

where u_S is the average dimerization of the soliton lattice [the maximum value of $|u_n|$ is $(\pi/2)u_S$], and K_S defines the periodicity and ϕ the phase of the soliton lattice distortion. The value of K_S is $2\pi/a'=0.4\pi/a$ for $y=20\%$. The limiting case of the undimerized chain is obtained with $u_S=0$.

We have, for simplicity, assumed in the calculations that $\phi=0$. In the real incommensurate case the phase has no effect on the total energy.

E. Numerical methods

We use a restricted basis set, which includes the hydrogen 1s and carbon 1s, 2s, 2p_x, 2p_y, and 2p_z orbitals.[45] The coefficients of the Gaussian expansion of the atomic crystal potentials $V_0^t(r)$ [Eq. (13)] are given in Table I. The fitting was performed in the same way as in Ref. 34.

For the calculation of $\Delta\rho$ [Eq. (9)] $11^3=1331$ reciprocal-lattice vectors were used. ΔE was decreased by about 100 meV with the number of $\mathbf{G}$'s increasing from 729 to the present number of 1331. The numerical integrations of the Fourier coefficients and $\Delta E_{\rm xc}$ were performed in a regular mesh containing $61\times41\times41\simeq10^5$ points in the primitive unit cell. This mesh division was optimized to give a practically converged ΔE versus u characteristics with a reasonable computing time. The larger number (61) mesh points in the polymer axis direction was found to be essential for obtaining $\Delta E(u)$ symmetrical with respect to the origin $u=0$. A smaller number (41) sufficed for other directions because the atoms move nearly parallel to the x-axis in the dimerization process.

The integrals in Eq. (29) were precomputed at 50 suitable discrete $R=|\mathbf{r}_p-\mathbf{r}_q|$ values in the range from $0.8a_0$ to $6.0a_0$ using $N=104$ Gaussian quadrature for the integrations (a_0 is the Bohr radius). The integration limit was cut to $12.0a_0$. The value at arbitrary R is interpolated using spline fitting. A suitable Gaussian quadrature was applied for the precalculation of the factors in the brackets in Eq. (27). Here the upper integration limit was set to $20.0a_0$. Although the pseudoatomic exchange-correlation energy is a constant, the numerical accuracy of the relatively small difference $\Delta E_{\rm xc}$ [Eq. (31)] was increased by integrating both parts in the same mesh of $61\times41\times41$ points. In the undoped case, the total charge of $\rho(\mathbf{r})$ is 14 per unit cell of a dimer C_2H_2, and $\Delta\rho(\mathbf{r})$ is electrically neutral. The numerical integration of $\Delta\rho$ in this mesh gave for $|\Delta\rho(\mathbf{G}=0)\Omega_0|$ less than 0.001 electrons. Cycle-dependent amounts (70–95 %) of the previous Fourier coefficients $\Delta V_C(\mathbf{G}_n)$ and $\Delta V_{\rm xc}(\mathbf{G}_n)$ were mixed into the new coefficients to improve the convergence during the SC iteration. The number of iteration cycles was 20. A much longer iteration changed ΔE by less than 2 meV per unit cell. We estimate that the numerical accuracy of our calculation is a few meV's.

In the study of the undoped chain we used three different k meshes in the one-dimensional Brillouin zone (BZ): (i) a regular mesh of 21 k's $[k/(\pi/a)=0.0,\pm0.1,\ldots,\pm0.9,\pm1.0]$ including the boundaries $k=\pm\pi/a$ (these two points with a half weight), (ii) a regular mesh of 20 k's $[k/(\pi/a)=\pm0.05,\pm0.15,\ldots,\pm0.85,\pm0.95]$ including only interior points, and (iii) a nonregular Gaussian mesh of 20 k's with the points and weights from the $N=20$ Gaussian quadrature, which has the last nodes at $k\simeq\pm0.993\pi/a$. The most accurate electron density and ΔE are obtained with the Gaussian mesh. Regular meshes of 11 k's (including the BZ boundaries with a half weight) and 10 k's (including only interior points) were also studied for drawing conclusions of the corvergence of ΔE with increasing number of k's.

In the study of the doped chain we used the regular mesh of 21 k's because it gives the dimerized ground state for the undoped chain with the same u_0 as the Gaussian mesh of 20 k's and allows us to study the effect of doping with a reasonable uniform accuracy. We did not use the Gaussian mesh in this case because the predetermined Gaussian mesh loses its better accuracy in the integration if the occupation of the states in the bands are modified. Furthermore, a more accurate estimate of the gap is obtained with the regular mesh of 21 k's because it includes the k point at the BZ boundary. The number of extra charge $|\delta N|$ ranged from 0.0 to 0.3 charges per unit cell, corresponding to a doping level $y=|\delta N|/2$ of 0–15 % per CH unit. Both electron ($\delta N>0$) and hole ($\delta N<0$) additions were treated.

TABLE I. Coefficients of the Gaussian expansion for V_0^t's of the SC LCGO calculations using the LDA. c_j and α_j denote the expansion coefficients and the exponents of the Gaussians, respectively [see Eq. (13)]. The corresponding coefficients $c_{j,H}$ and $\alpha_{j,H}$ of the pure Hartree calculations (the exchange-correlation fully neglected) are given in parenthesis.

Atom	j	c_j ($c_{j,H}$)	α_j ($\alpha_{j,H}$)
C	1	$Z=6$ ($Z=6$)	1.824 17 (1.657 3)
	2	2.000 62 (0.674 18)	37.690 78 (358.48)
	3	2.972 32 (2.801 0)	9.856 77 (44.418)
	4	6.112 12 (5.384 8)	3.003 03 (10.340)
	5	0.714 77 (6.580 6)	2.085 37 (2.589 1)
	6	−1.111 34 (−)	0.342 75 (−)
H	1	$Z=1$ ($Z=1$)	0.236 52 (0.352 72)
	2	0.501 88 (0.366 13)	0.748 59 (3.851 8)
	3	−0.014 17 (0.983 34)	0.103 47 (0.545 29)

The SC pure Hartree calculations (all exchange and correlation neglected at all stages) were performed parallel to the LDA calculations to study the effect of the local exchange correlation. We used the same basis set in the Hartree calculations as in the normal SC DF LDA calculations. The fits of the Gaussian expansion of V_0^i's for the Hartree calculations are given in Table I.

The calculations of the bands and total energies of the soliton and polaron lattices needing a large unit cell of $C_{10}H_{10}$ ($y=20\%$) were performed by using a regular mesh of 5 k's [$k/(\pi/a')=0.0,\pm0.5,\pm1.0$] (including the BZ boundaries with a half weight) in the new narrow BZ (the k points of this mesh coincide with the k points of the regular mesh of 21 k's of the smaller unit cell, if extended zone presentation is used), $5^3=125$ G vectors, and a regular mesh of $61\times21\times21$ points. The number of iteration cycles was 3. These calculations are therefore less accurate than those with the C_2H_2 primitive unit cell.

All the calculations were run on an IBM 3090 computer.

III. RESULTS AND DISCUSSION

A. Undoped chain

Although the band energies are *not* physically observable energies in the rigorous original HKS DF theory, one can use Janak's transition state argument[46] to perform approximate comparison. Our electronic band structures of undimerized ($u=0$) and dimerized [$u=0.026$ Å$\simeq u_0$(Exp.)] *trans*-polyacetylene calculated by using the regular mesh of 21 k's, are shown in Fig. 1. This particular k mesh was chosen here because it gives the band energies at the BZ boundaries and at $k=0$.

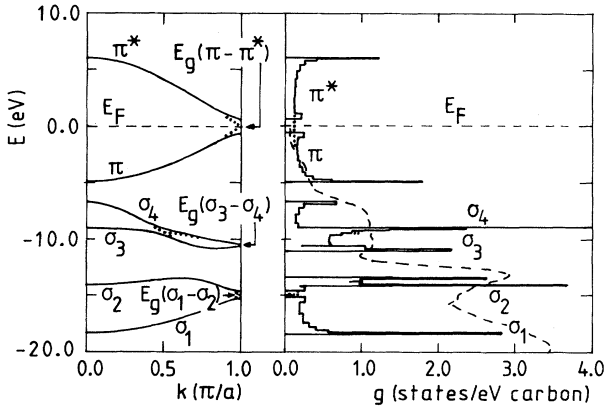

FIG. 1. Band structures of the dimerized ($u=0.026$ Å, solid line) and undimerized ($u=0$, dotted line) undoped *trans*-polyacetylene. $\sigma_1-\sigma_4$, π, and π^* denote the four deeper valence bands, the occupied bonding π band and the unoccupied antibonding π band, respectively. The corresponding densities of states are also shown. The zero energy is chosen to be in the middle of the π valence and π^* conduction band at the Fermi level E_F. Results are for the regular mesh of 21 k's. The dashed line represents the XPS spectrum of Keane *et al.* (Ref. 47) shifted down by 0.6 eV for comparison.

Note that the two deep degenerate core bands (c_1 and c_2) of carbon 1s character are not shown. The bands are labeled by the symbols $\sigma_1,\ldots,\sigma_4$, π (the uppermost occupied band), and π^* (the lowest unoccupied band). The $\sigma_1,\ldots,\sigma_4$ valence bands are basically formed via the sp^2 hybridization from the carbon 2s, 2p_x, and 2p_y orbitals as well as from the hydrogen 1s orbitals whereas the uppermost valence band and the lowest conduction band, the π and π^* bands, respectively, originate from the carbon 2p_z orbitals. The dimerization opens the gap $E_g(\pi-\pi^*)$ at the Fermi level E_F between the occupied π valence and unoccupied π^* conduction bands. $E_g(\pi-\pi^*)$ is much smaller than the total π band width $W\simeq11.0$ eV (defined as the energy difference between the π and π^* bands at $k=0$). Gaps are also opened between σ_1 and σ_2 bands and between σ_3 and σ_4 bands. The gaps $E_g(\sigma_1-\sigma_2)$ and $E_g(\pi-\pi^*)$ are linearly proportional to u: $E_g(\sigma_1-\sigma_2)\simeq20u$ eV/Å and $E_g(\pi-\pi^*)\simeq47u$ eV/Å (Fig. 2). The values of $E_g(\sigma_3-\sigma_4)$ are low and sublinearly proportional to u. Due to the improvements in computer codes and accuracy as well as the use of the improved approximation for exchange and correlation our new bands differ from the bands in Ref. 34 at some places a few eV's. The calculated DOS and the x-ray photoemission (XPS) spectrum by Keane *et al.*[47] are also shown in Fig. 1. The XPS spectrum is shifted by 0.6 eV downwards to facilitate a better comparison. Our DOS gives a natural explanation for the four bands of their XPS spectrum. The weak XPS structure in the range 0–5 eV can be associated with the π band DOS. The XPS band between 5 and 10 eV can be associated with the combined $\sigma_3+\sigma_4$ DOS. If the weak XPS shoulder above 5 eV could be associated with the onset peak of the σ_4 band in our DOS then the weak XPS peaks at 6.8 and 9.3 eV could naturally correspond to the σ_4 and σ_3 peaks of our DOS, respectively. The XPS peak at about 12 eV can be associated with the σ_2 peak of our DOS. Finally, the XPS peak at 18.7 eV can be associated with the σ_1 peak of our DOS, although here the double-ionization continuum may be involved in the XPS peak. Our inter-

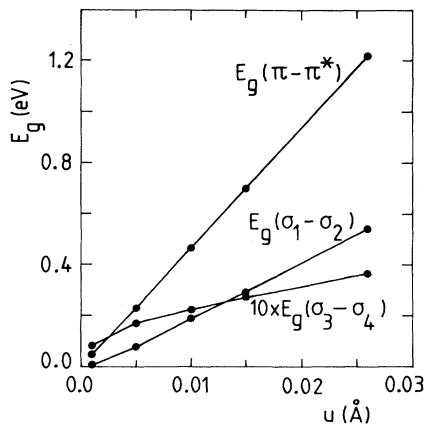

FIG. 2. Band gaps $E_g(\sigma_1-\sigma_2)$, $E_g(\sigma_3-\sigma_4)$, and $E_g(\pi-\pi^*)$ *at the BZ boundary* versus dimerization amplitude u. The small $E_g(\sigma_3-\sigma_4)$ has been scaled upwards by a factor of 10. Results are for the regular mesh of 21 k's.

pretation thus basically agrees with the interpretation given by Keane *et al.*[47] Also the positions of the peaks of our DOS agree with those of the XPS spectrum within an accuracy of about 1 eV.

The SC Hartree calculations neglecting all exchange and correlation at all stages give band structures which closely resemble the SC DF LDA bands. However, the core bands c_1 and c_2 are located at -221 eV below E_F in the SC Hartree case, compared with the value -258 eV in the SC DF LDA case.

The key quantities of various SC calculations are summarized in Table II. The band structures of the SC DF LDA calculations resemble each others. Especially σ_1, σ_2, π, and π^* bands are nearly identical. The most discernible differences are found in σ_3 and σ_4 bands in the region where the σ_3 and σ_4 bands are near the π valence-band minimum. In our calculation the σ_3 and σ_4 bands do not cross the π valence band. Our bands resemble most those of Ref. 48. Note that the bands obtained for a three-dimensional crystal should be wider and minimum gaps in the BZ narrower than those obtained for a single chain. This is the case with the results of Table II. The experimental ratio $E_g(\pi-\pi^*)/u_0$ is $\simeq 50-80$ eV/Å for the experimental gap of 1.4–1.8 eV (Ref. 3) and the experimental dimerization amplitude of 0.023–0.03 Å.[8–10] $E_g(\pi-\pi^*)$ is underestimated by about 30–70% in the SC DF LDA calculations, if the experimental geometry is assumed. This error is caused by the discontinuity Δ in the exact V_{xc} on addition of an electron,[49] which is not included in these SC DF LDA calculations (see also Ref. 17). On the other hand, the SC Hartree-Fock (HF) calculations give an overestimated gap of about 5–7 eV, but the inclusion of correlation decreases it.[50,51]

We have calculated the effective mass of a hole in the π valence band and the effective mass of an electron in the π^* conduction band as a function of u by fitting a parabola to the π and π^* band edges at the two largest $|k|$'s at the BZ boundary. The effective masses are shown in Fig. 3. The results for the Gaussian mesh of 20 k's are most accurate. The effective masses would probably approach zero with decreasing u, when the number of k's approaches infinity. If $u=0$, the $\pi-\pi^*$ gap vanishes, and the system becomes a simple metal with one π electron per CH unit in the metallic π band.

TABLE II. Key quantities of different self-consistent DF LDA calculations. The table gives the bandwidths and band gaps in eV. LCAO, LMTO, and PSP denote linear-combination-of-atomic-orbitals, linear-muffin-tin-orbital, and pseudopotential methods, respectively. 1D and *C* denote infinite single chain and crystal, respectively.

Method	LCAO[a]	LMTO[b]	PSP[c]	PSP[d]	LCGO[e]
"Dimensionality"	1D	1D	*C*	*C*	1D
$E_g(\pi-\pi^*)/u$ (eV/Å)	32	21	14	17	47
π valence band	4.9	4.1	4.5	5.1	4.4
π^* conduction band	4.7	$\simeq 5$	4.4	3.1	5.4
σ_1	3.7	4.1	3.7	4.0	3.2
σ_2	2.7	2.6	3.4	1.4	1.2
σ_3	3.1	3.6	2.8	1.7	1.8
σ_4	2.4	3.3	1.2	5.4	3.9
Gap $\sigma_1\rightarrow\sigma_2$	1.3	0.9	0.7	0.3	0.5
Gap $\sigma_2\rightarrow\sigma_3$	0.8	0.9	0.7	4.0	2.6
Gap $\sigma_4\rightarrow\pi$	-1.2	-1.3	0	-0.8	1.7

[a]Reference 14.
[b]Reference 13.
[c]Reference 17.
[d]Reference 48.
[e]This work.

Figure 4(a) shows the calculated electron density $\rho(\mathbf{r})$ at the polymer plane along the x axis and Fig. 4(b) the π electron density ρ_π at $z\simeq 0.458$ Å above the polymer plane where ρ_π is large. In the undimerized chain ($u=0$) the carbon-carbon bond lengths are equal and the electron density is the same in all bonds (the double bond is located at $x=0$ and the single bond at $x=\pm a/2$). The dimerization breaks this symmetry and results in an increase of the electron density in the (shorter) double bonds and a decrease of the electron density in the (longer) single bonds, a behavior which is clearly seen in Fig. 4 (compare the solid curve for $u=0.026$ Å with the dashed curve for $u=0.0$ Å). The π electron density $\rho_{\pi,k}=2|\Psi_{\pi,k}|^2$ at $z\simeq 0.458$ Å in the middle of the C—C and C=C π bonds versus wave vector k is shown in Fig. 5. The bonding π valence-band states increasingly contribute to the electron transfer from the single bonds to the double bonds when the BZ boundary is approached and/or when u is increased. The total contribution from the six other occupied bands, $\rho_k-\rho_{\pi,k}$, does not show any large variations as a function of k because of large cancellations.

The deformation part $\Delta\rho$ of the total electron density reflects the changes due to chemical bonding. The real part of the Fourier coefficient $\Delta\rho[G(1,0,0)]$

$$\mathrm{Re}\Delta\rho[G(1,0,0)]=\frac{1}{\Omega_0}\int_{\Omega_0}\Delta\rho(\mathbf{r})\cos\left[\frac{2\pi}{a}x\right]d^3r \qquad (35)$$

measures how much electrons are transferred from the

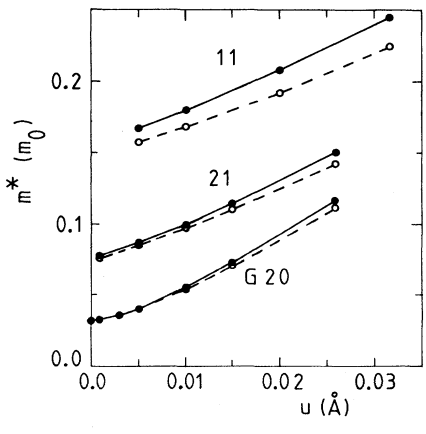

FIG. 3. Effective masses m^* of holes (solid lines) in the π valence band and of electrons (dashed lines) in the π^* conduction band. The symbols 21, *G*20, and 11 designate the regular mesh of 21 k's, the Gaussian mesh of 20 k's, and the regular mesh of 11 k's. m_0 is the mass of a free electron.

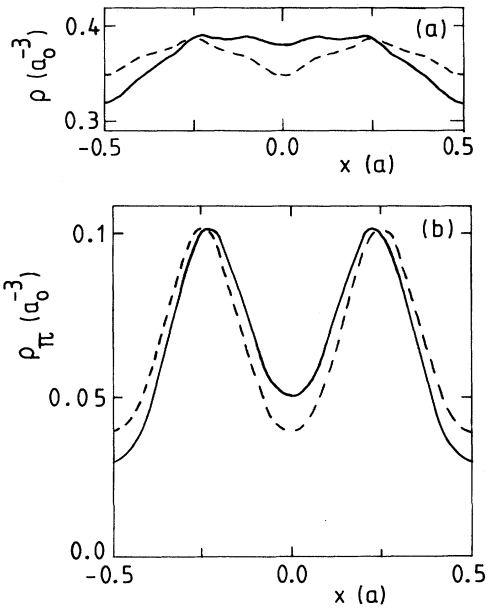

FIG. 4. (a) Electron density $\rho(\mathbf{r})$ along the polymer axis and (b) the π electron density ρ_π from the occupied π valence band along the line $y=0$, $z\simeq 0.458$ Å. The dashed line corresponds to $u=0$ and the solid line to $u=0.026$ Å. The results are for the Gaussian mesh of 20 k's.

region of the single bonds (around $x=\pm a/2$) to the region of the double bonds (around $x=0$). The imaginary part of $\Delta\rho[G(1,0,0)]$ is practically zero, as it should be because of the symmetry. The calculated $\mathrm{Re}\Delta\rho[G(1,0,0)]$, shown in Fig. 6, is found to be positive for $u>0$ and to increase with increasing u thus implying

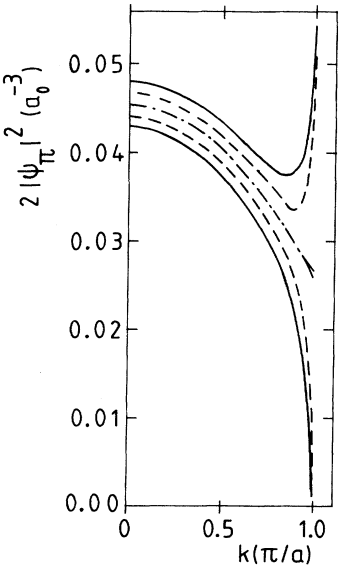

FIG. 5. $\rho_{\pi,k}=2|\Psi_{\pi,k}|^2$ vs k in the middle of the C—C (lower curves) and C=C (upper curves) π bonds at $z\simeq 0.458$ Å above the polymer plane. The dash-dotted, dashed, and full curves correspond to $u=0.0$, 0.005, and 0.01 Å, respectively. The results are for the Gaussian mesh of 20 k's.

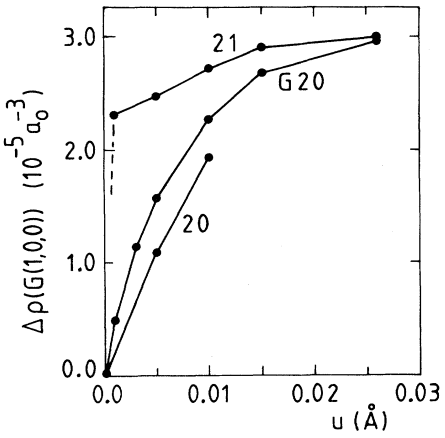

FIG. 6. Fourier coefficient $\Delta\rho[G(1,0,0)]$ vs dimerization amplitude u for the regular mesh of 21 k's, the regular mesh of 20 k's Γ, and the Gaussian mesh of 20 k's denoted in the figure by the symbols 21, 20, and $G20$, respectively.

electron accumulation in the double bonds. For the mesh of 21 k's $\mathrm{Re}\Delta\rho[G(1,0,0)]$ has a discontinuity at $u=0$ whereas for the two other k meshes this discontinuity is not present. The discontinuity comes from the π band and is entirely due to the $|\Psi_{\pi,k=\pm\pi/a}(\mathbf{r})|^2$ contribution to the double bonds.

The calculated total energy versus u for an undoped chain is shown in Fig. 7. Two different features are immediately obvious. (i) The total energy strongly increases with increasing u for $u>0.02$ Å. (ii) The results near the origin $u=0$ display a sensitive dependence on the k sampling. The curves corresponding to different k meshes approach each other at large dimerizations, but differ

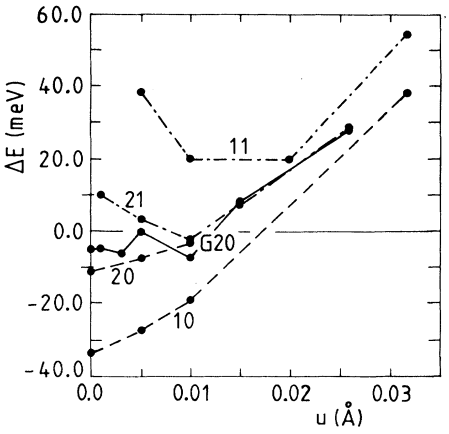

FIG. 7. Total energy ΔE per dimer C_2H_2 vs dimerization amplitude u for the regular mesh of 21 k's, the regular mesh of 20 k's, and the Gaussian mesh of 20 k's denoted in the figure by the symbols 21, 20, and $G20$, respectively. The total energies for the regular mesh of 11 k's and the regular mesh of 10 k's, denoted in the figure by the symbols 11 and 10, respectively, are also shown. The curves are only to guide the eye, and the same zero point has been chosen for all five cases.

considerably at small u's. ΔE(11 k's) and ΔE(10 k's) differ considerably from each others over the whole region $u=0-0.032$ Å studied. The better converged ΔE(20 k's) and ΔE(21 k's) differ for $u<0.01$ Å. ΔE(20 k's), neglecting the BZ boundary k's, gives an undimerized ground state, whereas ΔE(21 k's), overweighting the BZ boundary k's, gives a distinct minimum at $u=0.01$ Å. Here $\Delta E(u=0.001$ Å$)-\Delta E(u=0.01$ Å$)\simeq 12$ meV.[52] ΔE(Gaussian 20 k's) gives a weak minimum at $u=0.003$ Å and a distinct minimum at $u=0.01$ Å. However, due to the above sensitivity to k sampling we do not consider even ΔE(Gaussian 20 k's) to be very reliable for $u<0.005$ Å, and interpret ΔE(Gaussian 20 k's) to give a dimerized ground state at $u=0.01$ Å with $E_S\simeq 7$ meV, calculated here as the difference $\Delta E(u=0.005$ Å$)-\Delta E(u=0.01$ Å$)$. The carbon-carbon bond lengths corresponding to the dimerization of $u=u_0=0.01$ Å are $r_{C=C}\simeq 1.39$ Å and $r_{C-C}\simeq 1.42$ Å. Although we did not perform a full geometry optimization, we found that u_0 is rather insensitive to the bond lengths (and a) in reasonable limits: u_0 remains 0.01 Å, although E_S decreases from 18meV towards 0 meV and $r_{C=C}$ and r_{C-C} increase from about 1.37 to 1.41 Å and from 1.40 to 1.45 Å, respectively, when the unit cell length a and the x_n's are correspondingly scaled. Also the C—H bond direction chosen here is accurate enough for the present calculations.

According to experiments neutral *trans*-polyacetylene has a dimerized ground state with $u_0=u_0$(Exp.) $\simeq 0.023-0.03$ Å. The values of u_0 and E_S of SC DF LDA, SC HF, and SC correlated HF (CHF) calculations for infinite chains are given in Table III. The SC DF LDA calculations for infinite *trans*-polyacetylene single chains or crystals have resulted in u_0's ranging from 0 to 0.028 Å. Since our numerical accuracy is expected to be better than our calculated value $E_S\simeq 7$ meV at $u=u_0=0.01$ Å, we think that this minimum is real. Our results closely resemble those by Mintmire and White for a single *trans*-polyacetylene chain [$u_0\simeq 0.009$ Å, $E_S\simeq 6$ (3.5) meV].[15]. Although our small dimerization differs qualitatively from the zero dimerization by Ashkenazi *et al.*,[19] both calculations do find the extremely sensitive dependence of the results on the k sampling at the BZ boundary. In the light of the less converged results by Mintmire and White[15] ($E_S=42$ meV, $u_0=0.016$ Å for 11 k's including the BZ boundaries) and by us ($E_S\simeq 30-40$ meV, $u_0\simeq 0.015$ Å for 11 k's including the BZ boundaries) it seems that the calculations by Springborg *et al.*[13] [$E_S=56$ meV, $u_0=0.028$ Å$\simeq u_0$(Exp.) for 11 k's including the BZ boundaries] are similarly not fully converged and would give a weaker dimerization for a denser k sampling. Also the optimized C—C—C bond angle of 128° by Springborg *et al.* may favor dimerization. The molecular cluster study of $C_{20}H_{22}$ by Ye *et al.* results in a dimerized ground state with $u_0=0.035$ Å and $E_S=20-30$ meV.[53] The reason for this exceptionally larger u_0 is not clear to us but may be related to the finite size of the chain.

Since our results are in qualitative agreement with the Peierls mechanism[54]—the dimerization lowers the total energy and at the same time opens the gaps at the BZ boundaries—we adopt the common terminology used in the context of the Peierls mechanism in this paper. However, we *want to emphasize* that it is not possible to ascertain whether or not the Peierls mechanism is really at work here. This is due to the fact that the total HKS DF

TABLE III. Dimerization amplitude u_0 and dimerization stabilization energy E_S (per dimer C_2H_2) for different SC DF LDA, SC Hartree (*H*), SC Hartree-Fock (HF), and SC correlated HF (CHF) calculations (only the most recent results of the groups are given). LCAO, LMTO, LAPW, and PSP denote linear-combination-of-atomic-orbitals, linear-muffin-tin-orbital, linearized-augmented-plane-wave, and pseudopotential methods, respectively. 1D, *C*, EX, SP, and *G* denote single chain, crystal, exponential mesh, Monkhorst special points, and Gaussian mesh, respectively.

Authors (system)	Method	No. of k's	u_0 (Å)	E_S (meV)
Present work (1D)	DF LDA (LCGO)	20 *G*	0.01	7
Mintmire and White (1D)[a]	DF LDA (LCAO)	41 (∞)	0.009	6 (3.5)
Springborg *et al.* (1D)[b]	DF LDA (LMTO)	11	0.028	56
Ashkenazi *et al.* (1D, *C*)[c]	DF LDA (LAPW)	36 EX	$\simeq 0$	$\simeq 0$
Vogl and Campbell (*C*)[d]	DF LDA (PSP)	16 SP	0.005	
Ye *et al.* ($C_{20}H_{22}$)[e]	DF LDA (mol. cluster)		0.035	20–30
Present work (1D)	*H*	20 *G*	<0.005	
Suhai (1D)[f]	HF		0.0291	151
König and Stollhof (1D)[g]	HF		0.0328	$\simeq 120$
Suhai (1D)[f]	CHF		0.0238	86
König and Stollhof (1D)[g]	CHF		0.0252	$\simeq 80$
Experimental (*C*)[h]	x ray, NMR		0.023–0.03	

[a]Reference 15.
[b]Reference 13.
[c]Reference 19.
[d]Reference 17.
[e]Reference 53.
[f]Reference 50.
[g]Reference 51.
[h]References 8–10.

energy [Eq. (4)], when expressed in the alternative form using Eq. (2), is *not necessarily* a simple sum of band eigenvalues ε_j plus a strain energy E_S proportional to the leading order to u^2. Instead E_S may depend *nontrivially* on u via the Coulombic and exchange-correlation parts (see Ref. 19 as well as Mintmire and White and Ashkenazi *et al.* in Ref. 11).

Independently of the validity of the Peierls model for *trans*-polyacetylene the contributions from the BZ boundaries, especially from the π band states, are important for lowering the total energy and forming an electron density difference between the single and double bonds in the dimerization. It is therefore extremely important to sample the occupied π band at the BZ boundary carefully for obtaining the electron density and the total energy accurately.[15,18,19] Our results clearly show that inaccurate integration may even lead to qualitatively incorrect conclusions. According to the tight-binding argument[15,55] the absolute value of the error in our ΔE grows for small u proportionally to $N_k^{-2}\exp(-9N_k u/\text{Å})$ where N_k is the number of equidistant k points.[56] This sensitive behavior with respect to the k sampling should also be taken into account when calculating other conjugated polymers, especially when studying the ground-state geometry of the polymers which, like *trans*-polyacetylene, have a degenerate ground state.

There has been much debate about the origin of the dimerization of *trans*-polyacetylene (the relative importance of the electron-electron interactions and electron-phonon couplings).[11,13,15,17,19,51] These discussions are largely based on parametrized tight-binding model Hamiltonians, and it is not straightforward to analyze our first-principles results within such models. However, it is interesting to note in this context that the SC DF LDA $\Delta E_{xc}(u)$, shown in Fig. 8, is a decreasing function with increasing u for all k meshes thus significantly favoring dimerization. In comparison, the SC pure Hartree calculations neglecting all exchange and correlation at all stages resulted in a practically undimerized ground state with $u = u_0(\text{Hartree}) < 0.005$ Å, as shown in Fig. 9.

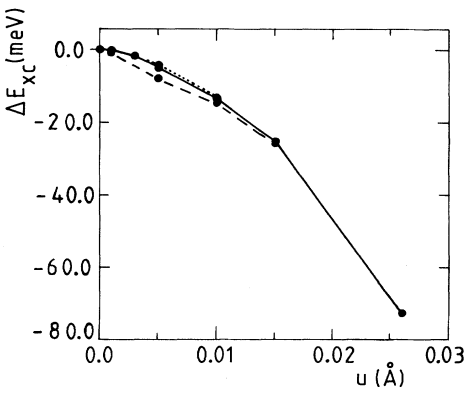

FIG. 8. Exchange-correlation energy ΔE_{xc} per dimer C_2H_2 vs the dimerization amplitude u. Dashed, dotted, and solid lines refer to the regular mesh of 21 k's, the regular mesh of 20 k's, and the Gaussian mesh of 20 k's, respectively. The same zero has been used for all three cases.

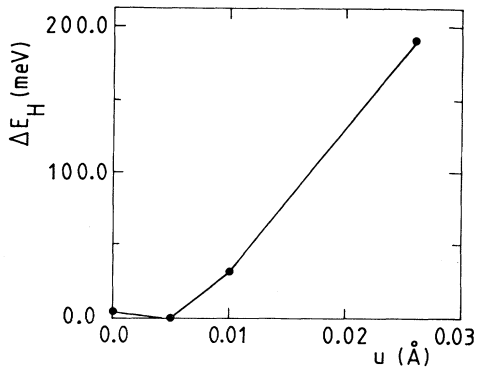

FIG. 9. Total energy of the pure Hartree calculations ΔE_H per dimer C_2H_2 vs u. These calculations neglected all exchange and correlation at all stages. The zero has been arbitrarily chosen. Results are for the Gaussian mesh of 20 k's.

However, because the calculated SC DF LDA $u_0 = 0.01$ Å $< u_0(\text{Exp.}) \simeq 0.023-0.03$ Å, we conclude that the local exchange correlation does not favor dimerization enough.

At this point it is also interesting to compare the above SC DF LDA and the SC pure Hartree result for infinite chains with the *ab initio* SC HF results. The SC HF calculations have a tendency to slightly overestimate the dimerization amplitude:[50,51,57] $u_0(\text{HF}) = 0.025-0.043$ Å as compared with the experimental value $u_0(\text{Exp.}) = 0.023-0.03$ Å. The size of the basis set has a strong effect on the HF results. A small basis set overestimates u_0 and E_S.[50] By comparing the results of our SC Hartree calculations [$u_0(\text{Hartree}) < 0.005$ Å] with the results of these HF calculations, it is obvious that the exact exchange strongly favors dimerization. However, the electron correlation effects are known to play an important role in the structural and optical properties (see, for example, Refs. 58 and 59). The proper inclusion of correlation in the HF calculations (CHF) reduces $u_0(\text{HF})$ of *trans*-polyacetylene by about 20%, bringing the dimerization amplitude inside the experimental range: $u_0(\text{CHF}) = 0.024-0.025$ Å.[50,51] Correlation reduces E_S quite remarkably by 40% from $E_S(\text{HF}) = 0.12-0.15$ eV to $E_S(\text{CHF}) = 0.08-0.09$ eV.[50,51] The proper inclusion of correlation to the HF calculations is therefore essential for obtaining quantitatively accurate values for u_0 and E_S.

B. Doped chain

We found that our calculated band structure of a uniformly dimerized chain with fixed u is only marginally modified by doping. We also found that $g(E_F)$ remains approximately constant equal to 0.12 states/eV/carbon atom in the undimerized case in the whole doping region $y = 0-15$ % studied.[33]

The calculated π electron density above the polymer plane in the center of the double and single bonds as a function of u for different doping levels y is shown in Fig. 10. Both doping by holes [Fig. 10(a)] and by electrons [Fig. 10(b)] strongly suppresses the charge-density wave

(the difference in the electron density between the double and single bonds). The calculated coefficient $\mathrm{Re}\Delta\rho[G(1,0,0)]$, measuring global changes in $\Delta\rho(\mathbf{r})$, is shown in Fig. 11. $\Delta\rho[G(1,0,0)]$ shows the same suppression of the charge-density wave under doping.[60] The effect of the occupied antibonding π^* states (unoccupied bonding π states) near the BZ boundary is to increase the single bond electron density (decrease the double bond electron density) and thereby decrease the differences between the bond charges. The discontinuity in the electron density at $u=0$ for small y's is due to the discretized k mesh.[18,33]

The total energy ΔE versus u for different doping levels y is shown in Fig. 12. Extra holes added into the polymer chain are expected to lead to a reduced dimerization, because the important states at the BZ boundary favoring dimerization become unoccupied. A corresponding effect may be expected for extra electrons, too, because the occupied π^* conduction band states at the BZ boundary should cancel the effect of the π valence-band states at the BZ boundary. In fact, the results of our total energy

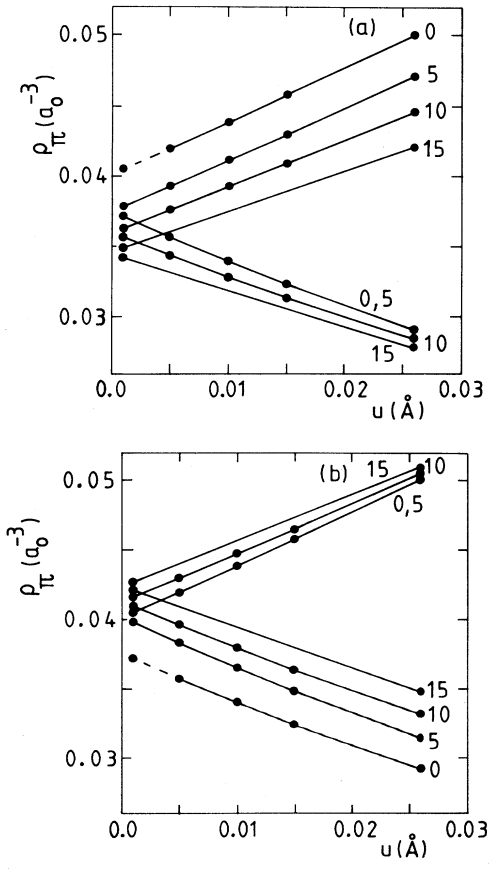

FIG. 10. π electron density ρ_π above the polymer plane between the carbon atoms in the double bond at (0,0, 0.0, $\simeq$0.458 Å) (rising curves) and in the single bond at ($a/2$, 0.0, $\simeq$0.458 Å) (descending curves) as a function of the dimerization amplitude u: for (a) extra holes and (b) extra electrons. The doping levels y (in percent per CH unit) are indicated in the figures. Results are for the regular mesh of 21 k's.

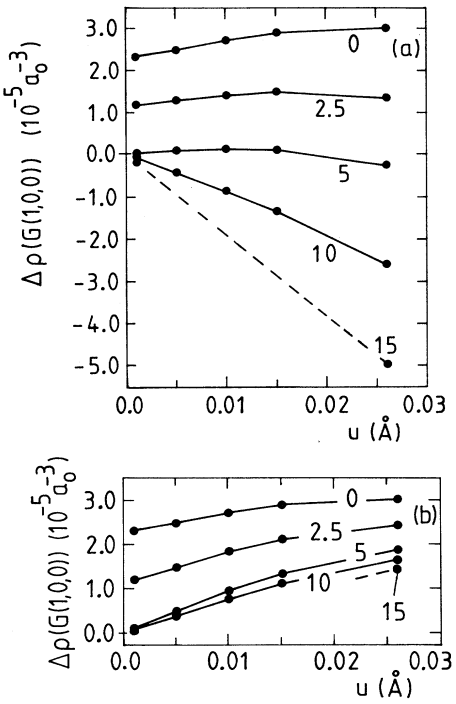

FIG. 11. Fourier coefficient $\Delta\rho[G(1,0,0)]$ vs dimerization amplitude u for different doping levels y for (a) extra holes and (b) extra electrons. The doping levels y are 0%, 2.5%, 5%, 10%, and 15% per CH unit (indicated in the figures). Results are for the regular mesh of 21 k's.

calculations, shown in Fig. 12, clearly confirm such a behavior. The dimerization, measured by the $u=u_0$ of the minimum of ΔE, becomes suppressed with increasing y. The $\pi-\pi^*$ gap at the BZ boundary $[E_g(\pi-\pi^*)]$ is proportional to u and therefore decreases with decreasing u_0. The transition from the semiconducting (semimetallic) state to the simple undimerized, gapless metallic state occurs (within our accuracy) at a critical concentration $y=y_c\simeq 4(3)\%$ per CH unit for extra holes (electrons). The doping has a large effect on the shape of the $\Delta E(u)$ curve at $y<y_c$ but a weaker further effect at $y>y_c$.

We estimate the zone-center optical-phonon frequency f_{opt} from the shape of the $\Delta E(u)$ curve around the ground state $u=u_0=0.01$ Å to be about 7×10^{13} Hz for undoped *trans*-polyacetylene. The commonly accepted value is about half of this.[1] f_{opt} is expected to attain a minimum value at $y\simeq y_c$, but increases again for $y>y_c$ up to about 5×10^{13} Hz (f_{opt} for $y>y_c$ is calculated around the undimerized ground state $u=u_0=0$).

We find that the shape of $\Delta E_{\mathrm{xc}}(u)$ is practically unaffected by extra charges in the range $y\leq 15\%$ although the absolute values are shifted due to the change in the total number of the electrons from the original 14 to $14+\delta N$ per unit cell. The local exchange correlation favors dimerization at all dopings, but its effect is not sensitive to the occupation of the π or π^* states at the BZ boundary.

The coupling between the dopant charges and the

chain geometry leads to the formation of self-localized states within the open, relatively large $\pi-\pi^*$ gap at low doping levels. Polarons and solitons (see, e.g., Ref. 1) are such self-localized states connected with a *local* reduction of the dimerization amplitude u from u_0 around the extra charge (the sign of u changes when passing through the soliton). The states are spatially separated by longer fully dimerized segments at low y's, and the system is therefore mostly commensurate, the solitons acting as local discommensuration centers.[5] Solitons are the energetically lower charge storage configuration than polarons but can be only created as soliton-antisoliton pairs.[1] Polarons do not have this restriction and may therefore be important if the charges are far from each others. Experiments indicate that the extra charge is mainly stored into solitons which gradually form a soliton lattice and a wider soliton band within the $\pi-\pi^*$ gap with increasing doping.[1] Due to the localized character of the states, the low effective mass of the band states (Fig. 3) is less meaningful in the lightly doped region because the charge is transported by hopping.

For a large number of extra holes or electrons, the dimerization stabilization energy and amplitude u_0 decrease, as shown in Fig. 12. According to our calculations, which assume uniform dimerization, a transition to a simple undimerized metallic state with $E_g(\pi-\pi^*)=0$ takes place at the critical doping level $y_c \simeq 4(3)\%$ for extra holes (electrons). An undimerized metallic state has a lower energy than a semimetallic uniformly dimerized state at $y > y_c$. Since the SC DF LDA calculations are known to underestimate u_0 (see Ref. 18 and references therein), the actual y_c should be somewhat larger. The use of a discretized k mesh brings also some inaccuracy to the exact value of y_c. Nevertheless, *we think that this qualitative change in the electronic structure has a close connection to the experimentally detected sharp increase in the Pauli susceptibility at* $y \simeq 6\%$.[4,5] The calculated DOS at the Fermi energy of the undimerized chain is $g(E_F) \simeq 0.12$ states/eV/carbon atom above our y_c, in fair agreement with the experimental value of $\simeq 0.08$ -0.12 states/eV/carbon atom in metallic *trans*-polyacetylene.[4-6]

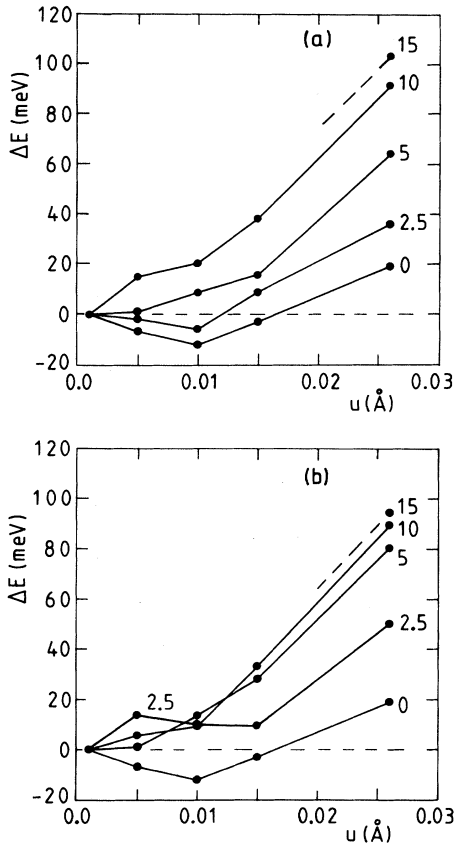

FIG. 12. Total energy ΔE per dimer C_2H_2 as a function of the dimerization amplitude u. The doping levels for (a) holes and (b) electrons are 0%, 2.5%, 5%,10%, and 15% per CH unit (indicated in the figures). The zero levels are arbitrarily chosen, and the lines are only to guide the eye. Results are for the regular mesh of 21 k's.

Our results, shown in Fig. 12, agree qualitatively with the HF and extended Hückel results of Refs. 61–64. The HF calculation by Tanaka *et al.*[63] gives the interesting behavior *dimerized lattice→soliton lattice→nearly undimerized lattice* with increasing y, although the last phase is obtained at a very high doping level of about 30%, and slight bond length differences and a gap at E_F are still present. However, the bond lengths are always found to become increasingly equal with increasing doping. Although we are not able to study the energy of a dilute soliton lattice with sufficient accuracy, we expect that the SC DF LDA calculations would also give the soliton lattice ground state for $0 < y \lesssim y_c$.

C. Polaron and soliton lattices

We considered above only the energy of the uniformly dimerized chain and not the other possible geometries such as polaron and soliton lattices, which have much larger unit cells and are therefore computationally more demanding. In fact, one possible model of the transition to the metallic state is that the soliton lattice, which is known to be the ground state at lower doping levels, dominates at high y's, too. The soliton lattice (a dense soliton lattice corresponds to an incommensurate Peierls state with a sinusoidal lattice and electron density distortion) has been supported in Refs. 5 and 24–29. The fact that an ordered one-dimensional soliton lattice has a gap at E_F, in disagreement with the first-order transitionlike rapid increase of $g(E_F)$ at $y \simeq 6\%$, motivated the polaron lattice model.[30,31] The polaron lattice has about the experimental $g(E_F)$. Furthermore, the infrared activities of polarons and solitons in the dilute concentration limit are nearly similar, a fact which was speculated to be generalizable to the highly doped state thereby explaining the persistence of the IRAV modes. According to the polaron lattice model, the spinless soliton lattice was expected to become unstable and a first-order transition to a polaron lattice to take place at $y \simeq 6\%$. However, the undimerized chain model[20,32,33] is the simplest way to explain the high $g(E_F)$. The persistence of the IRAV modes

above $y \simeq 6\%$ is often considered to be in disagreement with the undimerized chain but, also, with the polaron lattice because the resulting electron densities are nearly uniform in both cases and the infrared activity should be nearly totally quenched when passing from a dense soliton lattice to a polaron lattice or to an undimerized state.[25]

Our less accurate SC calculations for the sinusoidal polaron and soliton lattice distortions [see Eqs. (33) and (34)] with two holes per unit cell of $C_{10}H_{10}$ ($y = 20\% > y_c$) (two strongly interacting polarons or solitons per $C_{10}H_{10}$ unit) give (using the average dimerization amplitude 0.01 Å) the band structures presented in Figs. 13(b) and 13(c), respectively. Figure 13(a) shows the bands of the corresponding uniformly dimerized chain calculated with the same accuracy. The polaron lattice has two polaron bands (P_1 and P_2) and the soliton lattice one soliton band (S), respectively, in the π band region, in agreement with the general view.[1,31] At this high doping level above y_c these bands are quite wide. The band structures are very different from those expected for $y \ll y_c$ where the electronic structure is dominated by the large $\pi-\pi^*$ gap similar to that of the undoped chain, the polarons/solitons are far from each other, and the polaron/soliton bands in the $\pi-\pi^*$ gap are very narrow. Figure 14 shows the gaps in the π band region as a function of the average dimerization amplitudes u_{ave} ($u_{\text{ave}} = u$, u_P or u_S in the case of the uniformly dimerized chain, polaron lattice, or soliton lattice, respectively). The polaron lattice has two narrow gaps, $E_g(\text{VB}-P_1) \simeq 30 u_P A$ eV/Å and $E_g(P_2-\text{CB}) \simeq 13 u_P A$ eV/Å (VB and CB denote valence and conduction bands, respectively). The polaron bands in Fig. 13(b) correspond to an unrealistically large $A = 1.0$ chosen here to make $E_g(\text{VB}-P_1)$ and $E_g(P_2-\text{CB})$ more evident. In fact, these two gaps are the only clear difference between the bands of the polaron lattice and the uniformly dimerized state because the gap between the polaron bands is proportional to u_P, $E_g(P_1-P_2) \simeq 52 u_P$ eV/Å, and the gap $E_g(\pi-\pi^*) \simeq 52u$ eV/Å of the uniformly dimerized doped chain shows the same dependence on u.

The polaron lattice has the Fermi level in the middle of the polaron band [Fig. 13(b)] and therefore $g(E_F)$ has a large value of 0.125–0.144 states/eV/carbon atom. $g(E_F)$ of the polaron lattice increases with increasing u_P and A. The lowest value of 0.125 states/eV/carbon atom is obtained in the limiting case of the undimerized chain with $u_P \to 0$ and the highest value of 0.144 states/eV/carbon atom for $u_P = 0.026$ Å and $A = 1.0$. Although $g(E_F)$ of the polaron lattice is slightly larger than that of the undimerized chain or the experimental value of 0.08–0.12 states/eV/carbon, it is still in rough agreement with the experiments. On the other hand, the single chain soliton lattice has the Fermi level inside the gap producing a zero $g(E_F)$, clearly in disagreement with the experiments. The two gaps of the soliton lattice are linearly proportional to u_S: $E_g(\text{VB}-S) \simeq E_g(S-\text{CB}) \simeq 39 u_s$ eV/Å at $y = 20\%$ (Fig. 14). Notice that in the limit $y \ll y_c$ we would expect the soliton band width to be about zero and $E_g(\text{VB}-S) \simeq E_g(S-\text{CB}) \simeq E_g(\pi-\pi^*)/2$ where $E_g(\pi-\pi^*)$ is the gap of the undoped uniformly dimerized *trans*-polyacetylene chain.

The uniformly dimerized state is typically taken as the only possible ground-state geometry for the undoped *trans*-polyacetylene chain. Figure 15 shows the total energies for the undoped uniformly dimerized chain, undoped polaron lattice, and undoped soliton lattice versus the average dimerization amplitude u_{ave} with similar dis-

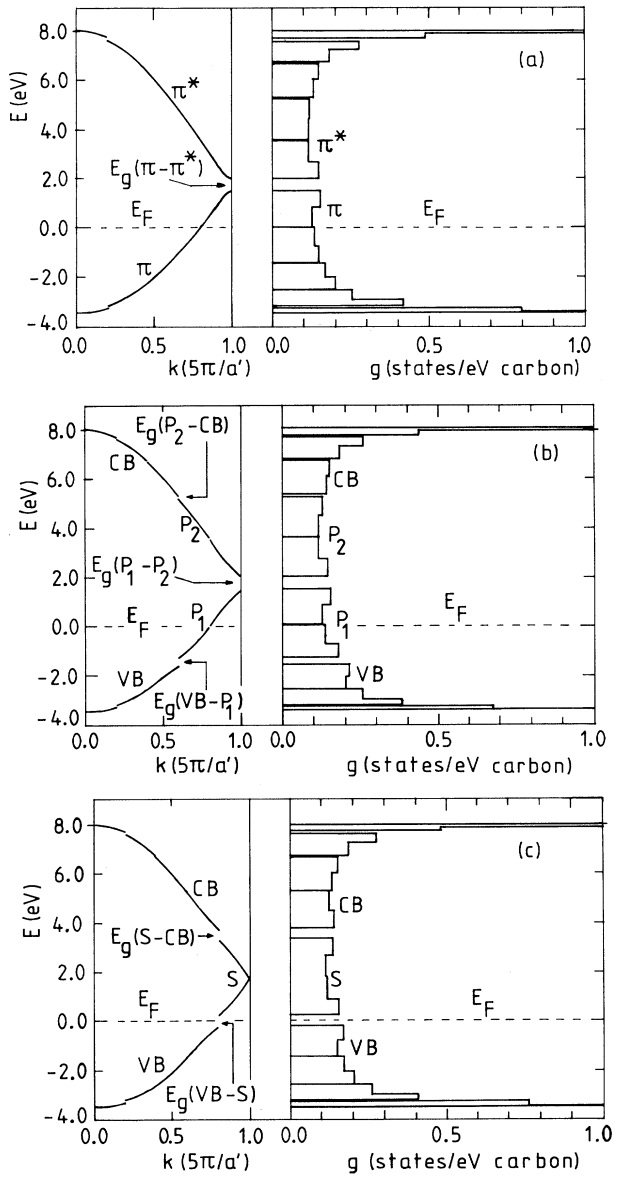

FIG. 13. Band structures of (a) a uniformly dimerized lattice for $u = 0.01$ Å, (b) a polaron lattice for $u_P = 0.01$ Å and $A = 1.0$, and (c) a soliton lattice for $u_S = 0.01$ Å. The hole doping level is $y = 20\%$ in all cases (two extra holes per $C_{10}H_{10}$) and an extended presentation has been used. P_1 P_2, S, VB, and CB designate the lower polaron band, the upper polaron band, the soliton band, the valence band, and the conduction band, respectively. E_F designates the Fermi level. The zero energy is set at E_F.

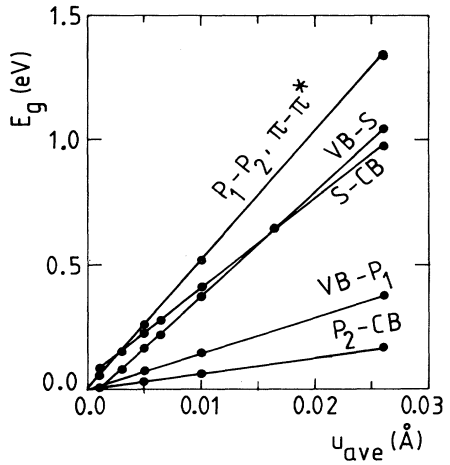

FIG. 14. $E_g(\pi-\pi^*)$, $E_g(P_1-P_2)$, $E_g(\mathrm{VB}-P_1)$, $E_g(P_2-\mathrm{CB})$, $E_g(\mathrm{VB}-S)$, and $E_g(S-\mathrm{CB})$ versus the average dimerization amplitudes u_{ave} ($u_{ave}=u,u_P,u_S$). The gaps of the polaron lattice are for $A=0.5$. For further information see the caption of Fig. 13.

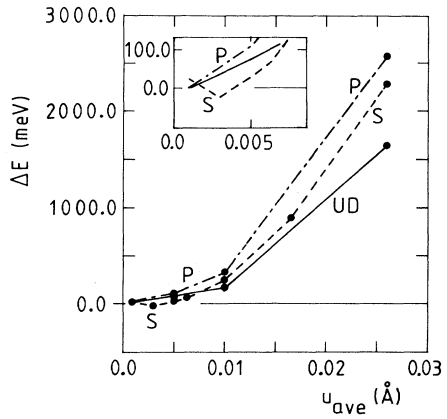

FIG. 16. Total energy per $C_{10}H_{10}$ unit for soliton (S) lattice, polaron (P) lattice ($A=0.5$), and uniformly dimerized (UD) chain doped with holes ($y=20\%$) versus the average dimerization amplitude u_{ave} ($u_{ave}=u_S,u_P,u$). To increase the numerical accuracy, the energies at $u_{ave}<0.01$ Å are averages of the total energies of negative and positive u_{ave}'s. The results are obtained by using a regular mesh of 5 k's (including the BZ boundaries).

tortions as used in the case of the doped lattices with $y=20\%$ below. The uniformly dimerized chain has the lowest energy. The undoped dense polaron and soliton lattices have larger energies which, furthermore, increase more steeply with increasing u_{ave}. The energy of the polaron lattice decreases when A decreases from 1.0 towards 0.0 for all u_P's (only the curve corresponding to $A=0.5$ is shown in Fig. 15). The ground-state geometry of the undoped *trans*-polyacetylene chain is thus uniformly dimerized with $u=u_0=0.01$ Å, in agreement with the more accurate results discussed earlier. Here the dimerization stabilization energy $E_S\simeq\Delta E(u=0.001$ Å$)-\Delta E(u=0.01$ Å$)\simeq 140$ meV per $C_{10}H_{10}$, or $\simeq 28$ meV per dimer.

The energy curves in the doped case $y=20\%>y_c$ are shown in Fig. 16. They differ considerably from those in Fig. 15. The curves corresponding to different lattices in Fig. 16 differ less from each other than the curves in Fig. 15. The energy of the polaron lattice (shown only for $A=0.5$ in Fig. 16) decreases with decreasing A for all u_P's and coincides at $A=0.0$ with the energy of the uniformly dimerized chain thus making the latter energetically more advantageous. Furthermore, the uniformly dimerized lattice attains its energy minimum for $u_{ave}=u=0$. The inset of Fig. 16 shows that the soliton lattice with the marginally small $u_S\simeq 0.003$ Å has a lower energy than the undimerized chain. However, this result is not definitive due to the reduced accuracy. By comparing the results of Figs. 15 and 7 we estimate that an accurate calculation would reduce the stabilization energy of this marginal soliton lattice of about 4 meV per dimer C_2H_2 in Fig. 16 below 2 meV per dimer C_2H_2, which is considerably less than the stabilization energy of the undoped uniformly dimerized chain (Fig. 7). The gap $E_g(\mathrm{VB}-S)$ at $u_S=0.003$ Å (corresponding to a maximum atom displacement $|u_n|$ of $(\pi/2)\times 0.003$ Å$\simeq 0.0047$ Å) is still open, and has a value of about 0.08 eV, but is considerably narrower than the gap $E_g(\pi-\pi^*)$ of about 0.5 eV of the undoped uniformly dimerized chain. The above energies for the soliton lattice are so small that interchain interactions, quantum fluctuations, thermal fluctuations, and thermal excitation of electrons across the gap may destroy the possible marginal soliton lattice.[14,20,30,65–68]

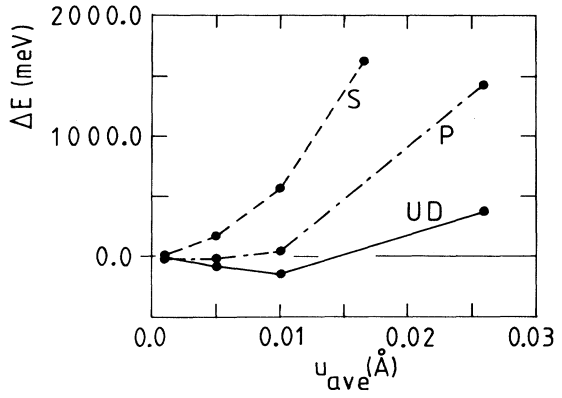

FIG. 15. Total energy per $C_{10}H_{10}$ unit for *undoped* soliton (S) lattice, polaron (P) lattice ($A=0.5$), and uniformly dimerized (UD) chain versus the average dimerization amplitude u_{ave} ($u_{ave}=u_S,u_P,u$). The results are obtained by using a regular mesh of 5 k's (including the BZ boundaries).

We consider next in more detail the different models suggested for the metallic state. The electronic bands of the polaron lattice [Eq. (33)] depend on the parameters u_P and A. According to our less accurate SC calculations, the gap between the two polaron bands, $E_g(P_1-P_2)$, is proportional to u_P, but not affected by A (Fig. 15). The small gaps between the polaron bands and the valence- or conduction band edges, $E_g(\mathrm{VB}-P_1)$ and

$E_g(P_2-\mathrm{CB})$, are proportional to $u_P A$. The electronic structure and the ground-state geometry of the polaron lattice should increasingly resemble those of the uniformly dimerized chain with increasing y, because the value of A should decrease as the polarons overlap more and more (see Ref. 25). In the limit $A \rightarrow 0$, the ground-state value of u_P, $u_{P,0}$, of the polaron lattice approaches u_0 of a doped uniformly dimerized chain. Our accurate results (Fig. 12) for the uniformly dimerized structure indicate that $u_0=0$ above y_c and therefore indirectly indicate that the possible polaronic lattice should also have a pronounced tendency to change into an undimerized metallic chain with increasing doping. Our less accurate calculations of different lattices using the unit cell of $C_{10}H_{10}$ for $y=20\%$ (Fig. 16) are in full agreement with the above considerations and indicate that the polaron lattice is unstable with respect to the undimerized chain. The study of Ref. 17 indicates that the interchain interactions, not included in our calculations but present in a three-dimensional crystal, make the storage of a single electron/hole charge into a self-localized polaron decreasingly favorable compared to the charge staying in the extended band states as the interaction strength increases. Although this result considers only noninteracting polarons in the limit $y=0$, we think that the interchain interactions should *not* increase the stability of the polaron lattice with respect to the undimerized chain in the highly doped state.

The band structure of the ordered soliton lattice has a gap at E_F [$g(E_F)=0$; see Figs. 13(c) and 14], which is expected to stabilize the soliton lattice with respect to the undimerized chain in the Peierls model. Experiments probing the DOS at E_F show no clear sign of a gap or a pseudogap at E_F, but indicate a *high density of extended states.*[4,6,7,20] The gap has thus to be eliminated by some mechanism. Disorder (possibly together with interchain interactions) could induce a finite density of states at E_F.[5,24,28,29] The study of Mele and Rice[24] indicates that the inclusion of both disorder and interchain couplings leads to a relatively smoothly increasing $g(E_F)$ versus y behavior for the insulator-metal transition in the doping range $y \simeq 2-10\%$. The effect of the interchain couplings, added on the disorder, is to weaken the soliton lattice distortion and to increase $g(E_F)$.[24] The resulting states at the Fermi level are considered to be localized because of disorder. However, the experiments show that *the high conductivity is based on good order, not disorder*[7,20] and the rapidity of the increase of the experimental Pauli spin susceptibility does not support disordered soliton lattice models.[4] Interchain couplings, if strong enough, may close the narrow gap. However, they are expected to weaken the soliton lattice distortion at the same time because the opening of a gap or, more generally, a pseudogap at E_F drives the incommensurate Peierls distortion. According to a recent study, the quantum fluctuations may also produce a nonzero $g(E_F)$,[68] but it is not clear whether the soliton lattice could survive the fluctuations. The studies of Refs. 69 and 70 indicate that, contrary to the common belief, disorder does not necessarily localize all states of a one-dimensional system, but the applicability of the random dimer model used in Ref. 69 to conjugated polymers was questioned.[71]

The results of the Takayama–Lin-Liu–Maki (TLM) model[72] for the energy difference between the uniformly fully dimerized and undimerized chains[25] are qualitatively in agreement with our results presented in Figs. 12 and 16, although the soliton lattice has always a lower energy than the undimerized state in the Su-Schrieffer-Heeger[73] (SSH) or TLM models. The SSH and TLM models take the electron-lattice coupling into account, but neglect electron-electron interactions which are known to be important (see, e.g., Ref. 11 and references therein). In the simplest approximation, the electron-electron interactions may be included by taking the on-site interaction term (Hubbard term) into account whereas the long-range interactions are neglected. In fact, such a one-dimensional Hubbard-Peierls model leads to a possibility of a gapless, undimerized metallic state at high doping levels while the soliton lattice is the ground state at low y's.[32] For reasonable parameter values a transition from the soliton lattice to the metallic state would take place at $y \simeq 3\%$,[32] in fair agreement with our value of y_c.

Approximating the real doping atoms by the uniform background charge, we are assuming that the dopants are evenly distributed and that a full charge transfer between the dopants and the polymer chain takes place. The NMR measurements on the alkali-metal (donor) -doped *trans*-polyacetylene indicate that the lithium and sodium dopants are in a purely ionic state but the situation is more complicated in the case of highly cesium-doped *trans*-polyacetylene.[74] On the other hand, the HF calculations of lithium-doped *trans*-polyacetylene indicate only partial charge transfer.[61] If the dopants were not completely ionized, our values of y_c should be scaled upwards. The presence of real acceptor or donor ions beside an undimerized chain might lead to chain compressions or stretchings (without bond alternations) around the ions with a further possibility to displacements perpendicular to the chain.[75]

The persistence of the doping-induced IRAV modes[23] is usually considered to be in agreement with the soliton lattice but in disagreement with the undimerized chain and the polaron lattice.[25,29] However, although the persistence of the IRAV modes indicates nonuniformities in the electron density, the connection to the soliton lattice is indirect.[20,22,67] It is thus not fully clear whether these nonuniformities at high doping levels are related to soliton (polaron) distortions or, for example, the screening charges induced by dopants. Although, as pointed out earlier, we think that disorder is *not* a precondition for the metallic state with a high $g(E_F)$ and high conductivity, thin barriers limiting the charge transport between relatively large and perfect metallic regions are still needed for explaining the experimental nonmetallic decrease of the conductivity with decreasing temperature.[7]

IV. CONCLUSIONS

To conclude, our self-consistent calculations for an undoped infinite single chain of *trans*-polyacetylene give a

weak dimerization with a dimerization amplitude of 0.01 Å, which is smaller than the experimental value by a factor 2–3, and a small dimerization stabilization energy of about 7 meV per dimer. Our calculations demonstrate the extreme sensitivity of the electron density and total energy to the k sampling near the Brillouin-zone boundaries for the small dimerization amplitudes which are relevant for the present study. The exchange-correlation energy clearly favors dimerization, but its effect is not large enough when the local-density approximation is used. We find that the undimerized metallic state becomes energetically more favorable than the uniformly dimerized state above a critical doping level of $y_c \simeq 4(3)\%$ for holes (electrons). Our method would probably give a soliton lattice ground state for $y < y_c$ although such calculations are beyond our present possibilities. According to our less accurate self-consistent calculations the undimerized state, or a marginal soliton lattice, is expected to be the ground state at high doping levels $y = 20\% > y_c$. The interchain interactions, quantum fluctuations, or thermal effects, not included here, may still destroy the possible marginal soliton lattice. Most properties of the metallic state, such as the high density of states at the Fermi level and the high conductivities, can be most naturally explained by a simple undimerized chain formed by a relatively rapid transition at $y \simeq y_c$ from a soliton lattice.

ACKNOWLEDGMENTS

The authors would like to thank Professor P. Kuivalainen for the early contribution to this work and illuminating discussions, and Dr. H. Stubb for his interest and encouragement during this work. The authors thank the Helsinki University of Technology for computer facilities. One of us (J.P.) was supported by the Technology Development Centre, Finland (TEKES).

[1]A. J. Heeger, S. Kivelson, J. R. Schrieffer, and W.-P. Su, Rev. Mod. Phys. **60**, 781 (1988); S. Roth and H. Bleier, Adv. Phys. **36**, 385 (1987); E. M. Conwell, IEEE Trans. Electr. Insul. **EI-22**, 591 (1987).

[2]H. Stubb, E. Punkka, and J. Paloheimo, Mater. Sci. Eng. R: Rep. **10**, 85 (1993).

[3]D. Moses, A. Feldblum, E. Ehrenfreund, A. J. Heeger, T. C. Chung, and A. G. MacDiarmid, Phys. Rev. B **26**, 3361 (1982).

[4]F. Moraes, J. Chen, T.-C. Chung, and A. J. Heeger, Synth. Met. **11**, 271 (1985); J. Chen and A. J. Heeger, *ibid.* **24**, 311 (1988).

[5]X. Q. Yang, D. B. Tanner, M. J. Rice, H. W. Gibson, A. Feldblum, and A. J. Epstein, Solid State Commun. **61**, 335 (1987).

[6]D. Moses, A. Denenstein, A. Pron, A. J. Heeger, and A. G. MacDiarmid, Solid State Commun. **36**, 219 (1980).

[7]A. B. Kaiser and S. C. Graham, Synth. Met. **36**, 367 (1990); Th. Schimmel, D. Gläser, M. Schwoerer, and H. Naarmann, in *Conjugated Polymers,* edited by J. L. Brédas and R. Silbey (Kluwer, Dordrecht, 1991), pp. 49–111; T. Ishiguro, H. Kaneko, Y. Nogami, H. Ishimoto, H. Nishiyama, J. Tsukamoto, A. Takahashi, M. Yamaura, T. Hagiwara, and K. Sato, Phys. Rev. Lett. **69**, 660 (1992); M. T. Ahmed, A. B. Kaiser, S. Roth, and M. D. Migahed, J. Phys. D **25**, 79 (1992).

[8]C. R. Fincher, C.-E. Chen, A. J. Heeger, A. G. MacDiarmid, and J. B. Hastings, Phys. Rev. Lett. **48**, 100 (1982).

[9]H. Kahlert, O. Leitner, and G. Leising, Synth. Met. **17**, 467 (1987).

[10]C. S. Yannoni and T. C. Clarke, Phys. Rev. Lett. **51**, 1191 (1983).

[11]S. Kivelson, W.-P.Su, J. R. Schrieffer, and A. J. Heeger, Phys. Rev. Lett. **58**, 1899 (1987); **60**, 72 (1988); C. Wu, X. Sun, and K. Nasu, *ibid.* **59**, 831 (1987); **63**, 2535 (1989); D. Baeriswyl, P. Horsch, and K. Maki, *ibid.* **60**, 70 (1988); J. T. Gammel and D. K. Campbell, *ibid.* **60**, 71 (1988); J. W. Mintmire and C. T. White, *ibid.* **63**, 2532 (1989); J. Ashkenazi, W. E. Pickett, H. Krakauer, C. S. Wang, B. M. Klein, and S. R. Chubb, *ibid.* **63**, 2533 (1989); J. L. Brédas and A. J. Heeger, *ibid.* **63**, 2534 (1989).

[12]M. Springborg, Phys. Rev. B **33**, 8475 (1986).

[13]M. Springborg, J.-L. Calais, O. Goscinski, and L. A. Eriksson, Phys. Rev. B **44**, 12713 (1991); Synth. Met. **41-43**, 3309 (1991).

[14]J. W. Mintmire and C. T. White, Phys. Rev. Lett. **50**, 101 (1983); Phys. Rev. B **28**, 3283 (1983).

[15]J. W. Mintmire and C. T. White, Phys. Rev. B **35**, 4180 (1987).

[16]J. Ashkenazi, W. E. Pickett, B. M. Klein, H. Krakauer, and C. S. Wang, Synth. Met. **21**, 301 (1987).

[17]P. Vogl and D. K. Campbell, Phys. Rev. Lett. **62**, 2012 (1989); Phys. Rev. B **41**, 12797 (1990).

[18]J. Paloheimo and J. von Boehm, Phys. Rev. B **46**, 4304 (1992); Synth. Met. **55-57**, 4443 (1993).

[19]J. Ashkenazi, W. E. Pickett, H. Krakauer, C. S. Wang, B. M. Klein, and S. R. Chubb, Phys. Rev. Lett. **62**, 2016 (1989); **63**, 1539(E) (1989).

[20]S. Kivelson and A. J. Heeger, Synth. Met. **22**, 371 (1988); G. Paasch, *ibid.* **51**, 7 (1992).

[21]G. Leising, Phys. Rev. B **38**, 10313 (1988).

[22]B. Horovitz, Solid State Commun. **41**, 729 (1982).

[23]D. B. Tanner, G. L. Doll, A. M. Rao, P. C. Eklund, G. A. Arbuckle, and A. G. MacDiarmid, Synth. Met. **28**, D141 (1989).

[24]E. J. Mele and M. J. Rice, Phys. Rev. B **23**, 5397 (1981).

[25]H.-Y. Choi and E. J. Mele, Phys. Rev. B **34**, 8750 (1986).

[26]E. M. Conwell, H. A. Mizes, and S. Jeyadev, Phys. Rev. B **40**, 1630 (1989).

[27]H. A. Mizes and E. M. Conwell, Phys. Rev. B **43**, 9053 (1991).

[28]S. Stafström, Phys. Rev. B **43**, 9158 (1991).

[29]S. Stafström, Phys. Rev. B **47**, 12 437 (1993).

[30]S. Kivelson and A. J. Heeger, Phys. Rev. Lett. **55**, 308 (1985); Synth. Met. **17**, 183 (1987); J. Voit and H. Büttner, Solid State Commun. **67**, 1233 (1988).

[31]S. Stafström and J. L. Brédas, Phys. Rev. B **38**, 4180 (1988).

[32]D. Baeriswyl, J. Carmelo, and K. Maki, Synth. Met. **21**, 271 (1987).

[33]J. Paloheimo and J. von Boehm, Solid State Commun. **87**, 487 (1993).

[34]J. von Boehm, P. Kuivalainen, and J.-L. Calais, Phys. Rev. B **35**, 8177 (1987).

[35]P. Hohenberg and W. Kohn, Phys. Rev. **136**, B864 (1964).

[36]W. Kohn and L. J. Sham, Phys. Rev. **140**, A1133 (1965).

[37]D. M. Ceperley and B. J. Alder, Phys. Rev. Lett. **45**, 566 (1980).

[38]J. P. Perdew and A. Zunger, Phys. Rev. B **23**, 5048 (1981).

[39]J. Avery, Int. J. Quantum Chem. **S13**, 403 (1979); **16**, 1265 (1979).

[40]J. Callaway and J. L. Fry, in *Computational Methods in Band Theory,* edited by P. M. Marcus, J. F. Janak, and A. R. Williams (Plenum, New York, 1972), p. 512.

[41]V. R. Saunders, in *Computational Techniques in Quantum Chemistry and Molecular Physics,* edited by G. H. F. Diercksen, B. T. Sutcliffe, and A. Veillard (Riedel, Dordrecht, 1975), p. 347.

[42]C. Hu and H. J. Monkhorst, Synth. Met. **40**, 369 (1991).

[43]C. Fredriksson and S. Stafström, Synth. Met. **41-43**, 3467 (1991).

[44]Note that in our paper the symbol a designates the length of *two* carbon-carbon bonds projected to the x axis. In the literature the symbol a often stands for the average projected *single* carbon-carbon bond length.

[45]R. Ditchfield, W. J. Hehre, and J. A. Pople, J. Chem. Phys. **54**, 724 (1971).

[46]J. F. Janak, Phys. Rev. B **18**, 7165 (1978).

[47]M. P. Keane, A. Naves de Brito, N. Correia, S. Svensson, L. Karlsson, B. Wannberg, U. Gelius, Sten Lunell, W. R. Salaneck, M. Lögdlund, D. B. Swanson, and A. G. MacDiarmid, Phys. Rev. B **45**, 6390 (1992).

[48]P. M. Grant and P. Batra, J. Phys. (Paris) C3-**44**, 437 (1983).

[49]R. W. Godby, M. Schlüter, and L. J. Sham, Phys. Rev. Lett. **56**, 2415 (1986).

[50]S. Suhai, Chem. Phys. Lett. **96**, 619 (1983); Phys. Rev. B **27**, 3506 (1983).

[51]G. König and G. Stollhof, Phys. Rev. Lett. **65**, 1239 (1990).

[52]For the mesh of 21 k's we got $\Delta E(u=0.0005\ \text{Å})=16$ meV and $\Delta E(u=0.0\ \text{Å})=37$ meV, which would indicate a steep increase for decreasing u. However, we omit these points because, differently from other points, their $\Delta\rho(\mathbf{r})$'s become asymmetric with respect to the origin.

[53]L. Ye, A. J. Freeman, D. E. Ellis, and B. Delley, Phys. Rev. B **40**, 6277 (1989).

[54]R. E. Peierls, *Quantum Theory of Solids* (Clarendon, Oxford, 1955).

[55]J. W. Mintmire and C. T. White, Int. J. Quantum Chem. Quantum Chem. Symp. **21**, 131 (1987).

[56]Note that our k mesh with an odd (even) number of k's equals (resembles) the mesh with an even (odd) number of k's in Refs. 15 and 55. For example, the mesh of 10 k's in Ref. 15 equals the regular mesh of 11 k's in our notation which has been used in this paper also when referring to the meshes in Ref. 15.

[57]A. Karpfen and J. Petkov, Solid State Commun. **29**, 251 (1979); Theor. Chim. Acta **53**, 65 (1979); A. Karpfen and R. Höller, Solid State Commun. **37**, 179 (1981); T. Yamabe, K. Tanaka, H. Terama-e, K. Fukui, A. Imamura, H. Shirakawa, and S. Ikeda, J. Phys. C **12**, L257 (1979); S. Suhai, J. Chem. Phys. **73**, 3843 (1980); H. Teramae, T. Yamabe, and A. Imamura, *ibid.* **81**, 3564 (1984).

[58]P. Fulde and G. Stollhoff, Int. J. Quantum Chem. **42**, 103 (1992).

[59]S. Suhai, Int. J. Quantum Chem. **42**, 193 (1992).

[60]The differences between the characteristics corresponding to hole and electron dopings in Fig. 11 are mostly due to the fact that the extra π electron charge δN of the doped systems is partly displaced with the carbon nucleus. Therefore $\Delta\rho[G(1,0,0)]$ of a doped chain becomes sensitive to the displacements of the nuclei, not only to the bond formation, resulting in an increasing negative (positive) contribution to $\Delta\rho[G(1,0,0)]$ for hole (electron) doping with increasing u.

[61]J. L. Brédas, R. R. Chance, and R. Silbey, J. Phys. Chem. **85**, 756 (1981).

[62]T. Yamabe, K. Tanaka, T. Koike, and M. Ueda, Mol. Cryst. Liq. Cryst. **117**, 185 (1985).

[63]K. Tanaka, M. Okada, T. Koike, and T. Yamabe, Synth. Met. **31**, 181 (1989).

[64]M. Kertész, F. Vonderviszt, and S. Pekker, Chem. Phys. Lett. **90**, 430 (1982).

[65]M. J. Rice and S. Strässler, Solid State Commun. **13**, 125 (1973).

[66]See Ashkenazi *et al.* in Ref. 11.

[67]S. A. Kivelson and M. I. Salkola, Synth. Met. **44**, 281 (1991).

[68]A. Takahashi, Phys. Rev. B **46**, 11 550 (1992).

[69]P. Phillips and H.-L. Wu, Science **252**, 1805 (1991).

[70]F. C. Lavarda, D. S. Galvao, and B. Laks, Synth. Met. **51**, 169 (1992).

[71]E. M. Conwell and H. A. Mizes, Synth. Met. **53**, 85 (1992).

[72]H. Takayama, Y. R. Lin-Liu, and K. Maki, Phys. Rev. B **21**, 2388 (1980).

[73]W. P. Su, J. R. Schrieffer, and A. J. Heeger, Phys. Rev. Lett. **42**, 1698 (1979); Phys. Rev. B **22**, 2099 (1980).

[74]P. Bernier, C. Fite, A. El-Khodary, F. Rachdi, K. Zniber, H. Bleier, and N. Coustel, Synth. Met. **37**, 41 (1990).

[75]D. S. Wallace, A. M. Stoneham, W. Hayes, A. J. Fisher, and A. Testa, J. Phys. Condens. Matter **3**, 3905 (1991).